Novel heme coordination variants of flavocytochrome P450 BM3

Hazel Mary Girvan, Helen Toogood, Rachael E Littleford, Harriet E Seward, W Ewen Smith, Idorenyin Ekanem, David Leys, Myles Cheesman, Andrew W Munro

Novel heme coordination variants of flavocytochrome P450 BM3

[1]Hazel M. Girvan*, [1]Helen S. Toogood, [2]Rachael E. Littleford, [3]Harriet E. Seward, [2]W. Ewen Smith, [1]Idorenyin Ekanem, [1]David Leys, [4]Myles R. Cheesman and [1]Andrew W. Munro*

[1]Manchester Interdisciplinary Biocentre, University of Manchester, Faculty of Life Sciences, 131 Princess Street, Manchester M1 7DN, UK. [2]Department of Pure & Applied Chemistry, University of Strathclyde, Thomas Graham Building, 295 Cathedral Street, Glasgow G1 1XL, UK. [3]Department of Biochemistry, University of Leicester, The Henry Wellcome Building, Lancaster Road, Leicester LE1 9HN, UK. [4]School of Chemical Sciences and Pharmacy, University of East Anglia, Norwich, NR4 7TJ, UK.

*Authors for correspondence: E mail Andrew.Munro@Manchester.ac.uk or Hazel.Girvan@Manchester.ac.uk. Phone 0044 161 306 5151; Fax 0044 161 306 8918

Running title: Novel P450 BM3 heme coordination mutants

These studies were funded by the Biotechnology and Biological Sciences Research Council (BBSRC, UK)

Abbreviations

CPR: Cytochrome P450 reductase; EPR: Electron Paramagnetic Resonance; MCD: Magnetic Circular Dichroism; P450: cytochrome P450 monooxygenase; P450 BM3 or BM3: Flavocytochrome P450 BM3 from *Bacillus megaterium*; RR: Resonance Raman spectroscopy. WT: wild-type.

Synopsis

Bacillus megaterium flavocytochrome P450 BM3 is a catalytically self-sufficient fatty acid hydroxylase formed by fusion of soluble NADPH-cytochrome P450 reductase and P450 domains. Selected mutations at residue 264 in the heme (P450) domain of the enzyme lead to novel amino acid 6th (distal) coordination ligands to the heme iron. The catalytic, spectroscopic and thermodynamic properties of the A264M, A264Q and A264C variants were determined in both the intact flavocytochromes and heme domains of P450 BM3. Crystal structures of the mutant heme domains demonstrate axial ligation of P450 heme iron by methionine and glutamine ligands *trans* to the cysteine thiolate, creating novel heme iron ligand sets in the A264M/Q variants. In contrast, the crystal structure of the A264C variant reveals no direct interaction between the introduced cysteine side chain and the heme, although EPR data indicate Cys264 interactions with heme iron in solution. The A264M heme potential is elevated by comparison to wild-type heme domain, and substrate binding to the A264Q heme domain results in a ~360 mV increase in potential. All mutant heme domains occupy the conformation adopted by the substrate-bound form of wild-type BM3, despite the absence of added substrate. The A264M mutant (which has higher lauric acid affinity than wild-type BM3) co-purifies with a structurally resolved lipid. These data demonstrate that a single mutation at residue A264 is enough to perturb the conformational equilibrium between substrate-free and substrate-bound P450 BM3, and provide firm structural and spectroscopic data for novel heme iron ligand sets unprecedented in nature.

Keywords

Cytochrome P450, P450 BM3, heme coordination, crystal structure, EPR, magnetic circular dichroism

INTRODUCTION

The cytochromes P450 (P450s) are a superfamily of monooxygenase enzymes responsible for a vast array of physiologically and biotechnologically important reactions in virtually all life forms [1,2]. Their catalytic repertoire includes such reactions as hydroxylation, dehalogenation, dehydration, reduction, epoxidation and isomerization [2,3]. Oxidative catalysis by P450s requires reduction of the resting (ferric) heme iron by two electrons; the first generating ferrous heme iron that binds molecular oxygen and the second reducing the ferrous oxy (or ferric superoxy) form to a ferric peroxy species. Successive protonations of this short-lived species generates the even more transient ferric hydroperoxy form (also known as compound 0) and (following its dehydration) the ferryl oxo (or compound 1) intermediate [4]. Compound 1 is considered to be the ultimate oxidant of the substrate in the vast majority of P450-dependent reactions, although it has proven elusive to isolation and characterization [5,6]. Recent cryogenic spectroscopic studies have, however, provided conclusive evidence for the formation of the compound 0 intermediate [7]. The electrons required for P450 catalysis are usually donated by NAD(P)H coenzymes and delivered to the P450 by one or more redox partner enzymes [6]. A typical mammalian P450 system consists of the FAD- and FMN-binding NADPH-dependent cytochrome P450 reductase (CPR) and the P450, both of which are membrane-bound proteins [8]. A typical prokaryotic P450 system (e.g. the *Pseudomonas putida* camphor hydroxylase P450cam) has soluble FAD-binding and NAD(P)H-dependent ferredoxin reductase, ferredoxin and P450 components [9]. However, it is now recognized that there is considerable biological diversity in the types of P450 redox apparatus. For example, P450 systems exist that have CPR fused to the P450, use pyruvate-dependent reductase partner proteins, or have dispensed altogether with redox partners in favour of direct interactions with peroxide or NAD(P)H [6,10].

One of the best characterized P450s, and an example of the class in which P450 and CPR-type enzymes are fused in a single polypeptide, is flavocytochrome P450 BM3 (BM3) from the soil bacterium *Bacillus megaterium* [11]. BM3 uses NADPH-derived electrons to catalyse hydroxylation of fatty acids, and has the highest monooxygenation rate yet reported for a P450 enzyme [12,13]. Protein engineering has been used extensively to explore structure/function relationships in BM3, to facilitate domain dissection and kinetic/thermodynamic characterization, and to modify its substrate recognition to enable oxidative catalysis of different substrates for biotechnological exploitation (e.g. alkanes and styrene [14-17]).

Factors for consideration in the exploitation of P450s for large scale production of oxyfunctionalized organic molecules is their inactivation by loss of heme iron ligation and/or displacement of the heme macrocycle altogether from the protein matrix [11,18]. In this respect, the demonstration that certain eukaryotic fatty acid hydroxylase P450s (CYP4 family) have their heme covalently attached (via a heme methyl group) to an acidic active site residue (usually glutamate) was an exciting discovery, and mechanistic studies demonstrated that the esterification reaction occurred in a P450-turnover dependent manner [19,20]. The possibility that increased heme stability could be imparted on other P450s by engineering a glutamate residue in the appropriate active site location was explored for the biotechnologically important P450cam and BM3 enzymes. A small amount of covalent linkage of heme-to-glutamate 248 through the heme 5-methyl group was induced through enzymatic turnover of a G248E mutant of P450cam, but this was not achieved for the comparable A264E mutant of BM3 [21,22]. However, in the case of BM3 the A264E mutant instead exhibited partial coordination of the Glu264 side chain as the distal ligand to the heme iron in the substrate-free form of the enzyme, and essentially complete Glu264 coordination in the substrate (fatty acid) bound form, with simultaneous retention of the cysteinate axial ligand (Cys400) on the proximal side of the heme [22,23]. In light of these data, we went on to create A264H/K mutants in the BM3 heme (P450) domain, where the His264 and Lys264 side chains that were shown to coordinate to the heme iron fully in both substrate-free and fatty acid-bound forms of the protein [24]. It was clearly established that point mutants at Ala264 offered the opportunity to create different types of heme iron ligand sets,

including variations not observed to date in nature. In this paper we describe the properties of A264M, A264C and A264Q mutants of BM3, exploiting spectroscopic methods and demonstrating further novel heme ligand sets. In addition, we characterize the status of the proximal heme ligand (thiol *versus* thiolate), the properties of the reduced A264M/C/Q/K/H/E enzymes are investigated for the first time, and crystal structures for the A264M/C/Q variants are presented for these novel heme coordination mutants. Our data reveal further new forms of proteinaceous heme coordination and spectroscopic signatures for these species.

EXPERIMENTAL

Mutagenesis, Gene Expression and Protein Purification

Generation of the A264K and A264H mutants in both heme domain and intact flavocytochrome constructs has been described elsewhere [24]. The A264C, A264M and A264Q mutations were each generated in both heme domain (pBM20) and flavocytochrome (pBM25) constructs using the Stratagene QuikChange mutagenesis kit. Primers used are described in the Supplementary Data section. Entire genes were sequenced to verify the presence of the desired mutation and confirm that no further unwanted mutations were present. The mutant and wild-type (WT) genes were expressed and proteins purified as described previously for both the heme (P450) domain and intact flavocytochrome forms of the enzyme [13,14,25].

Spectroscopic Analysis

Electronic absorption spectroscopy. UV-visible absorption spectra for the BM3 proteins were collected using a Cary 50 scanning spectrophotometer (Varian UK) and using a 1 cm path length quartz cuvette. Heme concentrations were calculated for each P450 mutant and WT protein using the pyridine hemochromagen method [26]. Spectra were collected for WT and mutant enzymes in the oxidised, dithionite reduced, reduced CO-bound, substrate-bound and inhibitor-bound states, as described previously [27]. Enzyme concentration for low-spin (LS) WT BM3 heme domain and flavocytochrome forms were determined spectrophotometrically using the previously established extinction coefficients of ε_{418} = 95 mM^{-1} cm^{-1} and 105 mM^{-1} cm^{-1}, respectively [13]. Binding of fatty acids and azole inhibitors to P450 BM3 and A264 variants was measured by spectral titration as described previously [22]. Binding titration data collection and fitting methods are described in greater detail in the Supplementary Data section.

Electronic Paramagnetic Resonance. Electronic Paramagnetic Resonance (EPR) spectra were collected using an EPR spectrometer comprising an ER200D electromagnet and microwave bridge interfaced to a EMX control system (Bruker Spectrospin), and fitted with a liquid helium flow cryostat (ESR-9, Oxford Instruments) and a dual-mode X-band cavity (Bruker type ER4116DM). Spectra were recorded for WT (400 μM), A264C (450 μM), A264M (520 μM) and A264Q (435 μM) heme domains in assay buffer at 10.8 K. EPR data for the A264E/K/H mutants were reported previously [22-24].

Magnetic Circular Dichroism. Magnetic Circular Dichroism (MCD) spectra were recorded using JASCO J/810 and J/730 dichrographs in the near UV-visible and near-IR regions, respectively, using an Oxford Instrument superconducting solenoid with a 25 mm ambient bore to generate a magnetic field of 6 Tesla. A 0.1 cm path length quartz cuvette was used to record near-IR spectra with sample concentrations the same as those used for EPR spectral collection. UV spectra were recorded for WT (30 μM), A264M (130 μM), A264Q (85 μM) and A264C (90 μM) heme domains with 50 mM HEPES in deuterium oxide (pH*, 7.0) as buffer (where pH* is the apparent pH measured in D_2O using a standard glass pH electrode).

Resonance Raman. Resonance Raman (RR) spectra were collected for substrate-free and arachidonate-bound (500 μM) WT, A264Q, A264M and A264C mutant heme domains (50 μM) at ambient temperature. A 15 mW 406.7 nm radiation source was used at the sample and delivered from a Coherent Innova 300 Krypton ion laser, with spectra acquired with a Renishaw micro-Raman system 100 spectrometer. The samples were held in a capillary under a microscope with 5 x 15 second exposures in each case.

Kinetic Studies and Product Analysis. Steady-state kinetic studies of P450 BM3 substrate-dependent NADPH oxidation were carried out with WT and each mutant flavocytochrome using arachidonic acid (arachidonate) and lauric acid (laurate) as substrates, as described previously [13]. Activities of the reductase domains of the flavocytochromes were analysed by cytochrome *c* reduction assays, as described previously [13]. Analysis of the turnover of laurate was done in 100 mM potassium phosphate (KPi), pH 7.0 at 25 °C using 400 nM WT and A264 mutant BM3 enzymes, 600 μM NADPH and 45 μM laurate with continuous stirring. Reactions were done in duplicate with control samples without enzyme added. Following complete oxidation of NADPH, the reaction mixture was adjusted to pH 2 by addition of 1 M HCl. Thereafter, lipids were extracted into dichloromethane and water removed by addition of solid magnesium sulfate. The filtered solution was then evaporated to dryness and the lipids dissolved in methanol, with sample analysis and quantification done using a Micromass Quatro triple quadrupole mass spectrometer (Manchester, UK), as described in our previous studies [28].

Potentiometric Analysis

Potentiometric titrations were carried out by the spectroelectrochemical method of Dutton and as described previously, with 6-10 μM enzyme in a 5 ml sample volume [29,30]. Redox potentiometry was carried out in a Belle technology (Portesham, UK) glove box under a nitrogen atmosphere and with oxygen levels maintained at less than 2 ppm. In order to remove residual traces of oxygen, protein samples were passed through a BioRad 10DG gel filtration column equilibrated with redox buffer (100 mM KPi, pH 7.0 containing 10 % glycerol). Potentiometry data collection and fitting methods are described in full in the Supplementary Data section.

Structural studies

The A264C, A264M and A264Q heme domains were crystallized by the sitting drop technique at 4 °C. Drops were prepared by addition of 2 μl of mother liquor to 2 μl 12 mg/ml protein solution in 10 mM Tris.HCl at pH 7.5. A264Q crystals were obtained with a mother liquor of 100 mM cacodylic acid pH 6.0, 160 mM $MgCl_2$ and 16 % PEG 3350. A264M crystals were obtained with mother liquor of 100 mM cacodylic acid pH6.0, 140 mM $MgCl_2$ and 18 % PEG 3350. A264C crystals were obtained under the same conditions, but with 100 mM $MgCl_2$. Crystals were flash frozen in liquid nitrogen using 10 % PEG 200 as cryoprotectant. Structures of the A264E/H/K mutants were reported previously [22-24].

Diffraction data for the A264C, M and Q mutants was collected on single flash-cooled crystals at ESRF ID14 beamlines. Data were analysed and merged using MOSFLM and SCALA [31]. The A264E structure was used as a starting model, with positional and B-factor refinement using REFMAC5 [32] alternated with manual model building cycles using COOT [33]. Final refinement and data collection statistics are given in Table 3 in Supplementary Data.

Materials

Restriction enzymes were from NEB (Herts, UK). Ampicillin, NADPH, yeast extract and tryptone were from Melford Labs (Suffolk, UK). DEAE Sepharose Fast Flow and Q-Sepharose was from GE

Healthcare (Uppsala, Sweden). Ceramic hydroxyapatite was from Bio-Rad Laboratories (California USA). PEG 3350 and PEG 200 were from Fluka. CO and NO were from BOC (Surrey, UK). All other reagents were purchased from Sigma Aldrich (Poole, UK) and were of the highest grade available.

RESULTS AND DISCUSSION

Expression and purification of P450 BM3 heme coordination variants

Previous studies of the P450 BM3 A264E variant indicated that this I-helix mutation did not significantly affect expression/purification of the mutant BM3 flavocytochrome or heme domains [22,23]. The A264C/H/K/M/Q heme domains and flavocytochromes were expressed in *E. coli* as described previously for WT P450 BM3 and the A264E variant [14,22,23]. A264M/C/Q mutations did not result in notable decreases in expression of the respective heme domains or flavocytochromes. The intact (flavocytochrome) forms of the A264K/H mutants were similarly unaffected. Enzymes were purified to homogeneity using chromatographic methods established for the WT enzyme (DEAE Sepharose, Q-Sepharose and hydroxyapatite resins). Protein yields were ~50 mg/litre for the heme domains and ~30 mg/litre for the intact enzymes. Concentration of the mutant P450s were determined as previously described, or using coefficients of 97, 113 and 98 mM^{-1} cm^{-1} for the A264Q/C/M proteins, respectively [13,24].

UV-visible absorption properties of P450 BM3 A264 mutants

Oxidised spectra: In all mutants, the heme spectral properties in the heme domains were indistinguishable from those of the flavocytochrome forms (i.e. those with appended diflavin reductase domain) and thus optical data described here pertain to heme domains. The UV-visible absorption spectrum of a P450 is a sensitive indicator of heme iron oxidation and spin-state, and is informative regarding changes in coordination of heme iron in the distal position (i.e. the loss of an axial water as the heme iron 6^{th} ligand, or its replacement with another ligand). Previous studies of the A264E variant indicated partial occupancy of the 6^{th} coordination position on the BM3 heme iron by the Glu264 side chain in the substrate-free enzyme (Soret maximum at 420.5 nm compared to ~418 nm for WT heme domain), and a near-complete conversion to a Cys-Fe-Glu ligand set on saturation with fatty acid substrates (Soret at 426 nm) [22]. The Soret maxima for the A264K/H mutants of the ferric heme domains are at 424/427 nm, respectively, consistent with complete distal coordination of the heme iron by the Lys/His264 side chains, as observed in the relevant heme domain crystal structures [24].

For the A264Q heme domain, spectral features of the oxidised, ligand-free enzyme were similar to those for WT BM3, with the Soret band at 418 nm, and α/β bands at 569/534 nm (compared to 569/535 nm for WT BM3), suggesting a WT-like coordination state of the heme iron. However, spectroscopic studies indicated at least partial coordination of heme iron by the Gln264 side chain and that similarities with the WT oxidised spectrum might originate from the nature of the novel ligation state (*i.e. via* the amide oxygen atom, *vide infra*). The A264C heme domain has a spectrum near-identical to that of WT heme domain, with maxima at 418 nm, 569 nm and 535 nm. A more pronounced shoulder on the low wavelength side of the Soret band (at ~390 nm) suggested a greater high-spin (HS) heme iron content than WT (Figure 1). The A264M heme domain exhibited spectral maxima at 416 nm, 566 nm and 534 nm. A more prominent shoulder (than WT) was again observed at ~390 nm, consistent with more HS ferric heme iron. This likely reflects dissociation of the distal water in a proportion of the A264C/M domains (Figure 1). The absence of a red shifted Soret band in the A264C/M mutants (as seen in A264K/H/E variants) does not suggest novel heme iron coordination states in these mutants. However, structural and spectroscopic studies indicated that, at least for the A264M mutant, the Met264 side chain coordinates the BM3 heme iron (*vide infra*).

Fatty acid substrate binding: Previous work showed fatty acid substrate-dependent formation of the Cys-Fe(III)-Glu ligand set in the A264E BM3 mutant [22]. Structural studies showed that, in substrate-free enzyme, the Glu264 side chain either (a) coordinates heme iron in the 6th position, or (b) interacts with the phenyl group of residue Phe87 in the pocket above the heme plane. Fatty acid binding displaces the Glu264 side chain from the Phe87 phenyl and results in near-complete coordination of the heme iron [22]. By contrast, fatty acid binding (e.g. arachidonate, palmitoleic acid [palmitoleate] or laurate) did not affect the (already hexacoordinated) ligation state of the A264K/H mutants. For A264Q heme domain, fatty acid binding resulted either in negligible optical perturbation (laurate) or in minor shifts indicating accumulation of HS heme iron (for palmitoleate and arachidonate). For longer chain fatty acids, the K_d values computed from optical titrations were similar to those for WT heme domain (e.g. 6.43 ± 0.51 μM for palmitoleate compared to 3.50 ± 0.17 μM for WT), despite much lower overall conversion to the HS form (Table 1). These data indicated retention of high substrate affinity in the A264Q mutant, but pointed to a less efficient 6th ligand displacement by lipid substrates, and hence the possibility that the Gln264 side chain coordinates the heme iron in a proportion of the molecules. For A264C heme domain, fatty acid-induced perturbation of the spin-state equilibrium was also observed in some cases, but extent of HS conversion was substantially less than observed for WT with arachidonate (K_d = 6.4 ± 0.3 μM compared to 0.55 ± 0.05 μM for WT) and palmitoleate, and negligible optical change was observed on titration with the saturated fatty acids palmitic acid (palmitate, C16), myristic acid (myristate, C14) or laurate (C12). For the A264M mutant, a more substantial fatty acid-induced HS conversion of heme iron was observed than for A264C, albeit slightly less than for WT with the same fatty acids. K_d determinations indicated a higher fatty acid affinity for A264M than for WT BM3 heme domain. For example, K_d values for A264M (WT) were 7.4 ± 0.4 μM (11.3 ± 0.4 μM) for palmitate, 0.9 ± 0.3 μM (6.9 ± 0.4 μM) for myristate, and 17.8 ± 0.9 μM (89.0 ± 15.0 μM) for laurate (Table 1). Thus, selected fatty acids were able to induce partial heme iron 6th ligand displacement for both the A264C/M mutants.

Inhibitor binding: To compare further the optical and ligand-binding features of WT and A264 mutant enzymes, we analysed the heme domain interactions with an inhibitory azole ligand that coordinates the heme iron in the 6th (axial) position. We chose 4-phenylimidazole (4-PIM); a small azole ligand with high affinity for P450 BM3 [22]. 4-PIM binding produced a Soret shift to 424 nm in WT heme domain, consistent with coordination of an imidazole nitrogen to the heme iron, and with a K_d = 0.84 ± 0.47 μM. The binding of 4-PIM is substantially stronger than for imidazole itself (535 ± 5 μM), consistent with our recent studies of binding of these ligands to the *Mycobacterium tuberculosis* CYP51B1 sterol demethylase P450 (K_d = 452 ± 27 μM for 4-PIM *versus* 11.7 ± 0.9 mM for imidazole) [34]. 4-PIM did not displace the endogenous amino acid 6th ligand in either A264H or A264K mutants. However, type II optical changes indicative of 4-PIM binding were observed for the other A264 mutants, consistent with the replacement of any aqua (or amino acid) ligand on the heme iron by the azole. For A264E heme domain, 4-PIM titration results in a Soret band shift to 426 nm (isosbestic point at 422 nm), with a K_d = 2.51 ± 0.49 μM. Our previous EPR studies indicated that the complex formed is homogeneous with 4-PIM completely coordinated to the heme iron [22]. For A264Q, the Soret shift is to 421 nm (isosbestic at 424 nm), with a K_d = 390 ± 27 μM; for A264C the shift is to 422.5 nm (isosbestic at 425.5 nm, K_d = 52.0 ± 2.8 μM); and for A264M the shift is to 420.5 nm (isosbestic at 424 nm, K_d = 440 ± 44 μM). 4-PIM is not highly soluble in aqueous solution, and turbidity develops at >2 mM. The 4-PIM K_d values for A264M/C/Q, while within this concentration range, report on only a partial conversion to the 4-PIM heme iron complex, as shown in Figure 2A for the A264C mutant. At higher 4-PIM concentrations (up to ~10 mM added), a distinct second phase of absorption change was

observed for the A264C/Q mutants, indicating a secondary binding event of lower affinity. No further significant absorption shift was observed for the A264M mutant in this range.

Gaseous ligand binding: WT heme domain shows near-complete conversion to a ferrous-CO (Fe(II)CO) complex with spectral maximum at ~448 nm following bubbling with CO gas in presence of sodium dithionite reductant. This confirms retention of a thiolate proximal ligand (from Cys400) in the Fe(II)CO complex, and negligible formation of a thiol-coordinated P420 species (Soret at 420 nm for BM3) [18,35]. Previous studies of A264K/H heme domains demonstrated negligible formation of a Fe(II)CO complex [24]. As discussed below, reduction of these domains to the ferrous form is feasible under anaerobic conditions, but the ferrous hemes retain their Lys/His distal ligands and there is no evidence for CO binding. By contrast, A264E heme domain underwent near-complete conversion to a Fe(II)CO complex with Soret maximum at 449 nm (P450 form), and only a small feature at 423 nm from a minor proportion (~10 %) of P420 [22].

The Fe(II)CO complex of A264Q heme domain (Figure 2B) has Soret maximum at 448 nm, (shifted from 418 nm in the ferric, water ligated state), indicating near-complete formation of the P450 form. For A264M the Fe(II)CO complex is again essentially completely P450 (Soret at 449 nm). For A264C, complete conversion to the Fe(II)CO species proved difficult, but the species formed was also almost completely P450 (Soret at 448 nm). None of the mutants exhibited any significant conversion of P450 to P420 (or *vice versa*) for up to 1 hour, indicating stability of the proximal thiolate ligand [34-36].

Ferric P450s are known to complex with nitric oxide (NO) to form Fe(III)NO (formally $Fe(II)NO^+$) adducts with distinctive spectral features [37]. For WT BM3 heme domain, the complex has its Soret band shifted to 434 nm, with complete conversion to the nitrosyl complex. The same is true for A264E heme domain (Soret at 435 nm) [22]. As for the CO binding data, NO complexes were not formed by A264K/H heme domains, and their endogenous amino acid 6^{th} ligands remained in place. However, NO complexes were formed for A264M/C/Q proteins, with Soret shifts to 435, 433 and 433.5 nm, respectively (see Figure 2B for A264Q-NO complex spectrum). Thus, NO can displace any endogenous 6^{th} ligand provided by the Met264, Cys264 or Gln264 amino acid side chains in the ferric forms of these enzymes.

Catalytic properties of A264 mutant flavocytochromes P450 BM3

To examine effects of A264 mutations on P450 BM3 catalytic properties, steady-state analysis of fatty acid-dependent NADPH oxidation was done (see *Experimental* section). Data for the reactions with laurate and arachidonate are presented in Table 1. Rate (k_{cat}) and apparent substrate affinity (K_m) constants for WT BM3 are consistent with previous values [e.g. 13,14], but k_{cat} values for all mutants were substantially lower than for WT. The kinetic constants for the A264K/H/C mutants were second order with respect to fatty acid concentration for both laurate and arachidonate. While this was expected for the A264K/H enzymes (where endogenous Lys/His ligands are not displaced on heme reduction), the data for the A264C variant were surprising in light of optical studies suggesting that the Cys264 side chain did not interact with heme iron, and that some substrate-dependent shift of heme iron spin-state equilibrium (towards HS) occurred on arachidonate binding. For the A264M mutant (where a more complete arachidonate-dependent spin-state shift was observed), the K_m value indicated high affinity for the fatty acid (10.3 μM), but k_{cat} was substantially lower than WT (115 min^{-1}). A264M turnover with laurate was also much slower than WT (k_{cat} = 195 min^{-1}), although K_m was also lower than WT (5.2 ± 0.8 μM). Apparent arachidonate affinity was also high for the A264Q flavocytochrome (K_m = 1.86 μM), and the k_{cat} rather higher than for other mutants described here (754 min^{-1}). However, A264Q-catalysed laurate turnover was also second order with respect to fatty acid concentration, albeit with a superior rate constant to that for the A264K/H/C mutants (Table 1). Collectively, data

demonstrate clearly that fatty acid oxidation is compromised in all A264 mutants, and that the position of the relevant 264 amino acid side chain (even in enzymes or sub-populations thereof where the residue does not ligate the heme iron) likely interferes with catalytically productive substrate docking. Steady-state cytochrome *c* reduction (requiring electron transfer from FMN, and hence preceding reactions of FAD reduction by NADPH and inter-flavin electron transfer) was investigated for all mutant flavocytochromes, and at near-saturating concentrations of NADPH (500 μM) and cytochrome *c* (200 μM). In all cases, rates of >100 s^{-1} were determined, consistent with the value previously determined for the WT BM3 (k_{cat} = 109 ± 4 s^{-1}), and demonstrating clearly that electron transport from NADPH through to the FMN cofactor (reduction of cytochrome *c* occurs near-exclusively from the FMN) is not significantly affected in A264 mutant reductase domains and thus cannot explain decreased fatty acid oxidation kinetics [12].

To establish that fatty acid-stimulated electron transfer in WT and A264 mutant flavocytochromes was linked to substrate hydroxylation, products from turnover of laurate were characterized. For WT BM3, all substrate was converted to mono-hydroxylated products (ω-1 to ω-3 hydroxylation of laurate), as described previously [38]. Under the same conditions, small amounts of the same hydroxylaurate products were obtained from A264Q (~5 % product formed), A264E (~8 %) and A264M (~5 %) mutants, while approximately 20 % product formation was observed for A264C. Thus, most product formation was observed for the A264C flavocytochrome, in which there appears to be no heme iron coordination by Cys264. Despite a slow rate of substrate-dependent NADPH oxidation, a substantially higher proportion of product is formed in this mutant, possibly due to less steric interference with fatty acid docking close to the heme by the relatively small Cys264 side chain (compared to Q/E/M264 residues). Levels of product formation in the A264M/C/Q/E mutants thus do not correlate with extent of spin-state perturbation induced by fatty acid binding (although formation of HS heme iron was previously correlated with a favourable shift in WT BM3 heme iron potential and electron transfer to the heme iron [38]), or with the apparent k_{cat} values with laurate. Thus, it is concluded that laurate hydroxylation is much more uncoupled from NADPH oxidation in the A264M/Q/E mutants than in A264C, despite A264C's much lower rate of fatty acid-stimulated NADPH oxidation. In turn, A264C is substantially more uncoupled than WT BM3. The A264K/H mutants are inactive fatty acid hydroxylases, consistent with other studies showing that the Lys/His264 side chains are not displaced by substrate binding or heme reduction.

Potentiometric studies on A264 mutants

To establish heme iron midpoint reduction potential for the A264 mutants, and to assess whether substrate-dependent modulation of heme iron potential occurs (as in WT BM3), spectroelectrochemical titrations of both ligand-free and arachidonate-bound heme domains were done, as previously [13,30]. Consistent with previous data, a substantial increase (109 mV) in heme potential was determined for arachidonate-bound WT heme domain [30,39]. This elevation of potential (probably together with structural reorganization) likely facilitates FMN-to-heme electron transfer in the substrate-bound flavocytochrome [11]. For the A264C/Q heme domains, arachidonate binding also induces large increases in HS ferric heme iron content. The heme redox potentials for substrate-free A264Q and A264C heme domains were identical, within error, to that for WT, and arachidonate binding induced large increases in heme potential in both cases (361 mV and 145 mV, respectively, Table 2). The reduced states of substrate-free and arachidonate-bound forms of the A264Q/C mutants have Soret maxima at 410/411 nm, respectively (Figure 3). These absorption values are similar to that for WT BM3 heme domain and indicate retention of thiolate coordination in the ferrous state. For A264C, the redox potential change is of similar magnitude to that for WT BM3 heme domain [30,39], but the increase in potential for A264Q is substantially greater than determined previously for WT or other P450 BM3 mutants.

The redox potential for A264M in the substrate-free form was also substantially more positive than for WT heme domain (by 172 mV), and was not perturbed significantly by arachidonate binding, even though there was substantially greater HS heme iron content in the arachidonate-bound form of the ferric A264M domain than in the substrate-free form (Table 2, Figure 3). In substrate-free A264M, the reduced species has a Soret maximum at 410 nm and a distinct shoulder at 435 nm, with two visible region bands at 539 nm and 562 nm. The ferrous arachidonate-bound A264M mutant has its maxima at the same wavelengths as the substrate-free reduced form, but with decreased Soret intensity at 410 nm, and increased relative intensity in the 435 nm shoulder. The 410 nm Soret band is assigned to a ferrous, pentacoordinated cysteine thiolate-bound heme iron, as seen for WT heme domain. We tentatively assign the 435 nm species to a hexacoordinated Met-Fe(II)-Cys thiolate species.

For A264K/H heme domains, spectra observed on maximal achievable reduction with sodium dithionite (*ca* 70 %) differ significantly from WT enzyme. Ferrous A264H mutant has its Soret at 428 nm, with visible region bands at 558/530 nm. Both bands are more intense than their ferric counterpart. These features correlate well with spectra from Perera *et al*., which were attributed to thiol ligation to heme iron in their studies of the ferrous myoglobin H94G cavity mutant with neutral thiol/thioether sulfur donor ligands [35]. Thus, we conclude that ferrous A264H heme domain has His-Fe(II)-Cys thiol coordination. The ferrous A264K heme domain also differs substantially from WT. The Soret maximum is shifted to 424 nm, with a proportion at 445 nm, and with three distinct visible region bands at 529, 558 and 568 nm. The species with Soret at 424 nm correlates with the A264H data (and with pK_a titration, see below), indicating Lys-Fe(II)-Cys thiol coordination for this proportion of the enzyme. The 445 nm species is attributed to a Lys-Fe(II)-Cys thiolate coordinated form.

To clarify the nature of the mixed species observed in the ferrous A264K mutant, a pK_a titration was performed. Enzyme, in an anaerobic environment, was reduced with sodium dithionite at pH 5.5 prior to titration with NaOH. The starting spectrum collected at pH 5.5 had its Soret at 423 nm, with a small shoulder at 445 nm, and with visible region bands at 565/536 nm. Elevation of pH resulted in a marked increase in intensity of the long wavelength Soret shoulder, accompanied by decreased intensity of the 423 nm band. Visible region features shifted to 557/524 nm. We consider that the spectral shift observed for ferrous A264K reflects conversion from a species with near complete thiol proximal coordination (at pH 5.5) to one with mixed thiol/thiolate coordination at pH 9. The conversion was reversible and pH dependence of spectral changes was fitted using the Henderson-Hasselbalch equation to give a pK_a value of 6.50 ± 0.04 (Figure 4). Thus, reversible protonation/deprotonation of the 5th ligand was observed, as seen in our previous work on CYP121 [36].

Spectroscopic analysis of BM3 A264 variants

Spectroscopic studies of the A264 mutant heme domains were done to define more clearly the nature of heme iron coordination in the solution states of the proteins, and to enable firm conclusions to be drawn relating to any differences between heme iron coordination states in solution and crystal forms.

EPR analysis: EPR spectroscopy reports on the spin state of ferric heme iron, and on the nature and orientation of heme iron ligands. For the various BM3 A264 mutants, EPR could provide important data confirming, or otherwise, the presence of novel amino acid side chain ligands to the heme iron and proportions of such species populated. Previous studies confirmed fatty acid substrate-dependent coordination of A264E BM3 heme iron by Glu264, and substrate-independent coordination by His264 and Lys264 in A264H/K mutants [22-24]. EPR spectra for WT and A264M/C/Q heme domains are overlaid in Figure 5. The g-values for all A264 mutants are presented in Table 1 in the Supplementary Data, and compared to those for the A264E mutant and for WT BM3 heme domain in ligand-free and ligand-bound states.

For A264Q, the EPR spectrum is consistent with a LS ferric heme species. The g-values were distinct from those for WT BM3 heme domain, with features at 2.48 (g_z), 2.25 (g_y) and 1.90 (g_x), compared to 2.42, 2.26 and 1.92 for WT BM3. The g-values for A264Q are similar to those for A264K, which also contains a single set of rhombic features at 2.47, 2.26 and 1.91, thus suggesting that Gln264 occupies the 6th ligand position on the heme iron in A264Q under these conditions (i.e. at 10 K) [22]. While these data cannot categorically define the nature of the ligating atom as an amide oxygen or nitrogen from the Gln264 side chain, it is likely to be the oxygen (see below).

For the A264M domain, there is a complex mixture of signals, indicating both HS and LS heme species (see Figure 5 legend). A minor HS species occurs with g-values at 7.98, 3.62 and 1.71, and is assigned to a pentacoordinated heme iron with a cysteinate 5th ligand and the 6th aqua ligand displaced. Of the four LS species visible, the one with g-values at 2.43, 2.25 and 1.92 is similar to that for the substrate-free WT domain, and is thus assigned to a hexacoordinated LS species with water as 6th ligand. The species with g-values at 2.53, 2.25 and 1.89, and at 2.47, 2.25 and 1.92 are assigned to novel LS hemes with Cys-Fe-Met ligation. These assignments are consistent with previous EPR assignments for P450cam in complex with sulfur donor ligands [40]. Specifically, g-values of 2.5, 2.27 and 1.89 were observed for P450cam bound to dimethylsulfide, compared to 2.42, 2.25 and 1.92 for the dimethyl disulfide complex, and 2.44, 2.25 and 1.91 for the aqua-coordinated, LS resting form [40]. A further set of A264M g-values is observed at 2.39, 2.25 and 1.98. Similar heterogeneity (i.e. three distinct LS, cysteinate-coordinated species) was observed previously in studies of P450cam bound to 1-propanethiol [40]. Addition of substrate (arachidonate, 500 μM) to the A264M mutant provided data further consistent with these assignments, with a decreased complexity of the EPR signal, and an increase in the HS component (with g_z at 7.98) at the expense of the aqua-coordinated component (with g_z at 2.43). EPR signals are sensitive to the orientation as well as to the nature of heme iron ligands. Thus, the complex mixture of A264M LS species may be a consequence of different orientations of the distal thioether and/or proximal cysteinate ligands. Since orientation of the cysteinate is conserved in crystal structures of WT and all A264 mutants, we consider heterogeneity of the distal ligand position to be more likely in A264M.

For the A264C domain, there is also a more complex population of species than in WT heme domain (Figure 5). Apart from the component assigned to LS, aqua coordinated (2.42, 2.25 and 1.92) and a small proportion of HS 5-coordinated heme iron (g-values as for the comparable A264M species), there are other sets of g-values (specifically 2.47, 2.25 and 1.91, and 2.37, 2.25 and 1.94) that suggest interactions between the Cys264 side chain and the heme iron. The species with g_z at 2.37 is comparable to that for P450cam in complex with the dithiothreitol anion, and thus suggests *bis*-thiolate coordination of BM3 heme iron [40]. The species with g_z at 2.42 is comparable with EPR features for the β-mercaptoethanol- and methanethiol-bound forms of the cysteinate-coordinated *Caldariomyces fumago* chloroperoxidase enzyme, and for propanethiol-bound P450cam, and may thus relate to species with thiol distal coordination [40,41]. However, EPR data indicative of Cys264 interaction with heme iron in A264C are at odds with crystal structural data, and possible explanations are considered in more detail below.

MCD studies: MCD is an important tool for characterizing iron coordination in hemoproteins [42]. MCD spectra were recorded in both near UV-visible (300-700 nm) and near infrared (NIR, 700-1400 nm) regions to obtain further data on heme coordination states of A264 mutants. In particular, the position of a LS porphyrin-to-ferric heme iron charge-transfer (CT) band in the NIR MCD region is an important reporter of alterations to heme ligation state [43].

Near UV-visible MCD spectra for WT and A264M/C/Q mutants are shown in Figure S1 in Supplementary Data. These reveal differences in band positions and intensities between WT and A264 mutants. Thiolate (i.e. cysteinate) coordination is indicated by the relative band positions and their low intensities compared to those for other LS hemoproteins with different coordinating ligand(s). For the

A264Q/C mutants, the heme is predominantly LS (as for WT BM3) with CT_2 bands at 575.9 nm/577.1 nm, compared to 575.7 nm for WT BM3. By contrast (and as observed in the electronic absorption spectra), the A264M mutant has the CT_2 band shifted to 573.5 nm, consistent with a considerable proportion of HS heme iron. Differences consistent with a greater proportion of HS heme in A264M are also evident from the derivative feature in the 600-700 nm range. WT and A264C/Q mutants have minima between 656.5-657.5 nm, but the A264M minimum is shifted to 645.5 nm, and is of much greater intensity than for WT and the other mutants. In the NIR MCD region, the CT_{LS} peak is an important marker for heme iron coordination state. In WT heme domain the peak is at 1077 nm, consistent with previous studies [22,44]. The CT_{LS} peak is also at 1077 nm for A264C, but is shifted to 1084/1086 nm for the A264M/Q mutants, respectively (Figure S1 in Supplementary Data). As can be seen for the substrate-bound, HS form of WT BM3 heme domain, the CT_{LS} band is considerably diminished in intensity, with development of a CT band at ~835 nm. A small HS feature is also observed for A264C, and the A264M variant has a larger amount of the HS feature, again consistent with optical studies. Conclusions from these room temperature MCD studies are that there is possibly little heme iron coordination by Cys264 in the A264C variant, but that both Met264 and Glu264 ligate, at least in a proportion of the enzyme, in the respective A264M/Q mutants. For A264M (again consistent with other spectroscopic studies reported here), there is evidence for both pentacoordinate HS and hexacoordinate LS species, all with cysteinate as proximal ligand. There are clearly two hexacoordinate forms, which we assign to either Met264 or water ligated in the distal position. For the A264Q mutant, MCD studies demonstrate an almost exclusively LS heme, with retention of the cysteinate proximal ligand and either water or Gln264 in the distal position. The position of the NIR CT_{LS} band is at ~1086 nm for A264Q. In previous studies of the A264E mutant, this feature shifted from 1080 nm (partial occupancy of Glu264 as 6th heme ligand) to 1085 nm in the arachidonate-bound form, where arachidonate binding induced a near-completed switch to a Cys-Fe(III)-Glu heme iron ligand set [22,23]. The similar position of this feature in A264Q is consistent with a considerable proportion of this enzyme adopting a Cys-Fe(III)-Gln ligand set, and would also suggest that the amide oxygen atom of Gln264 is the 6th ligand to the heme iron.

Resonance Raman characterization: Resonance Raman (RR) spectroscopy provides important information on vibrational frequencies of bonds within a P450 heme, and reports on heme iron oxidation, spin and coordination states [45,46]. Data were collected for A264 mutant heme domains with laser excitation at 406 nm, close to the Soret maximum. In all cases, the ν_4 oxidation state marker band was centred at 1371/1372 cm^{-1}, consistent with previous studies on WT BM3 heme domain and confirmatory of ferric heme iron in each A264 mutant [14]. In all cases, substrate (arachidonate, 500 μM) binding did not alter the ν_4 position, confirming retention of ferric heme iron. The ν_3 feature is a convenient heme iron spin-state marker band, and for WT BM3 heme domain is resolved by curve fitting into two features at 1481 cm^{-1} (HS) and 1500 cm^{-1} (LS), with the LS species predominant [47,48]. On substrate addition, the balance changes in favour of the HS ν_3 species, consistent with optical data. The A264K/H mutants have ν_3 at 1495 cm^{-1} in both substrate-free and arachidonate-bound forms, confirming retention of the LS state and the nitrogenous 6th ligand in the substrate-bound ferric forms. A264Q heme domain in its substrate-free state has a major ν_3 feature at 1500 cm^{-1}, but a small shoulder develops at 1480 cm^{-1} on arachidonate binding, indicative of a minor proportion of HS heme iron and consistent with optical titration data. For A264M, ν_3 features are at 1482 cm^{-1} (minor) and 1500 cm^{-1} (major) for the as-purified protein, with these features becoming roughly equal in intensity for arachidonate-bound protein. Structural data for A264M heme domain indicate that some fatty acid remains bound through the purification process (see below), consistent with the RR data here and with A264M K_d values for fatty acid binding being lower than those for WT (Table 1). For A264C, ν_3 values are ~1501 cm^{-1} for substrate-free heme domain, with (as for WT) a shift in equilibrium towards

a 1482 cm^{-1} species on arachidonate binding. Collectively, RR data confirm that WT and all A264 mutants are thiolate-coordinated, ferric proteins in their resting state, and that all but A264M are predominantly LS in absence of exogenous substrate. Arachidonate binding also leads to accumulation of 5-coordinate HS signals for the A264C/Q mutants. Other RR features reporting on perturbations to heme ring planarity and conformations of heme substituent groups are discussed further in the Supplementary Data section. RR spectra for WT and the A264M/C/Q/K/H mutants are shown in Figure S2 in the Supplementary Data, and frequencies and intensities of the key vibrational bands are annotated in Supplementary Data Table S2.

Structural analysis of A264M, A264Q and A264C heme domains

Studies of the BM3 A264E/K heme domains revealed that both substrate-free (SF) and palmitoleate-bound forms of these mutants crystallized in a conformation previously considered as that populated by WT BM3 in its substrate-bound (SB) form [23,24]. The lower K_d values determined for fatty acid binding to A264E (compared to WT BM3) suggested that the SB conformation adopted by this mutant was that with higher affinity for fatty acids (as opposed to substrate binding to the SF form and then inducing a conformational "switch") [22]. Structural studies of the A264H mutant showed this heme domain occupied the SF conformation (see Figure S3 in Supplementary Data). This conformation was the only one compatible with distal coordination of heme iron by the His264 side chain [24]. Here, we crystallized the A264M/C/Q heme domains, and collected x-ray diffraction data to a resolution of 2.5 Å, 2.1 Å and 2.0 Å, respectively. All crystallized in the same space group ($P2_12_12_1$) as the previously determined A264E/K heme domains, and were in the SB conformation [23,24]. Data collection and final refinement statistics for the new mutant structures are presented in Supplementary Data Table S3.

Analysis of heme environment in the A264M heme domain demonstrated clearly that the Met264 side chain coordinated the heme iron, creating a novel hexacoordinated Cys-Fe-Met protein (Figure 6). Our data are consistent with spectroscopic studies and confirm that this unprecedented heme iron ligand set exists in both solution and crystal states of A264M heme domain. EPR (at 10 K) and room temperature optical studies indicate that both "Met264-on" forms (i.e. those where Met264 ligates the heme iron), a pentacoordinate HS species and a hexacoordinate aqua-coordinated LS form exist in equilibrium. The predominance of the "Met264-on" forms in solution is the likely reason for the apparent complete Met264 coordination observed in the crystal structure, as minor species are unlikely to be detected at the resolution obtained. The complexity of the LS A264M EPR spectrum originates from distinctive species that include a water-ligated species, but possibly also from species with different orientations of the Met264 ligand or oxidative modification of its sulfur atom. It is conceivable that reductive activation of the A264M P450 intracellularly leads to oxidation of the Met264 sulfur by transient catalytic cycle oxy-intermediates in a proportion of the protein.

In agreement with low fatty acid K_d values for A264M, there was clear electron density corresponding to a bound fatty acid substrate in one of the two molecules in the asymmetric unit. This was modelled as palmitate, consistent with previous work demonstrating co-purification of palmitate with two other fatty acid hydroxylases purified from *E. coli*; namely *Bacillus subtilis* P450 BioI (CYP107H1) and the peroxide driven $P450_{BS\beta}$ from the same bacterium [28,49]. The ω-terminal region of the bound fatty acid interacts with the Phe87 side chain, as seen for palmitoleate-bound WT BM3 heme domain [50]. However, for both molecules in the asymmetric unit, heme iron ligation by the methionine and overall protein conformation are identical and thus appear independent of the presence of the fatty acid. From optical spectra, the purified A264M flavocytochrome had a HS content similar to that of the A264M heme domain, confirming high affinity for fatty acids is retained in intact A264M enzyme.

The crystal structure of the A264C heme domain shows the Cys264 side chain above the heme plane, within van der Waals distance of both Phe87 and the 6th water ligand (Figure 6). It makes no stable hydrogen bonding interactions with any other residue or water molecules and there was no

evidence of oxidation of the cysteine thiol from the electron density. The picture of a single ligation state, as observed for both A264C heme domains in the asymmetric unit, is somewhat at odds with the complexity and heterogeneity of the EPR spectrum. It is possible that the alternative species are only minor populations within the crystal, making their detection difficult. These alternative forms could correspond to various oxidised forms of the Cys264 sulfur (e.g. sulfenic, sulfinic or sulfonic forms) created following sulfur reactions with oxy-heme intermediates. Each of these species could contact the heme iron or its 6th aqua ligand and perturb the EPR signal. Oxygen atoms from putative oxidised cysteine species may also be disordered in crystals, further complicating their detection. While direct Cys264 ligation of heme iron might occur in solution, this would require major structural reorganization of the protein. However, the plasticity of the BM3 heme domain is well known from preceding structural studies [22-24]. Similar to most A264 mutants, both A264C heme domains within the asymmetric unit are in the SB conformation, although no fatty acid substrate was detected in either molecule in this case.

In contrast to the A264M/C mutants, that show no significant heterogeneity in ligation state in the crystal structures, dual occupancy for the Gln264 side chain in the A264Q mutant was observed (Figure 6). These conformations correspond to "Gln-on" and "Gln-off" states, with respect to coordination of the heme iron by the Gln264 side chain. This is analogous to the situation for the A264E mutant, as the Gln-off state has the Gln264 side chain interacting with the Phe87 side chain [22,23]. Similar to the A264E mutant, we have modelled the Gln-on state as ligating through the amide oxygen. This assignment remains tentative on the basis of x-ray crystallographic data alone (which cannot distinguish between oxygen or nitrogen ligation at this resolution). EPR data are similarly inconclusive, since there is no evidence of any line splitting that could be indicative of a nitrogen ligand. As for previously determined hemoprotein structures with amide ligands, e.g. the pentacoordinated H175Q mutant of cytochrome *c* peroxidase (CCP) and the hexacoordinated *Rhodobacter sphaeroides* SHP hemoprotein (*Sphaeroides* heme protein), we have modelled A264Q ligation to occur via the oxygen atom, similar to known ligation patterns of amide compounds with hemes [51,52]. Coordination of heme iron by nitrogen in the BM3 A264Q mutant would require deprotonation of the amide nitrogen [50]. SHP is the only known naturally occurring example of a heme amide ligation. In this case, the heme iron axial ligands are His47 and Asn88. In ferric SHP, the Asn88 amide coordinates the heme iron, but on reduction this 6th ligand dissociates to leave a pentacoordinated ferrous heme iron bound only by a His47 axial ligand [52]. Our data for the BM3 A264Q mutant are thus the first reporting a hexacoordinate amide-ligated heme with cysteinate as the 5th ligand, and the first example of a hexacordinated heme protein with glutamine as an axial ligand. In the Gln-off state, a water molecule replaces the Gln264 amide as heme 6th ligand. The A264Q heme domain is also in the SB conformation, but again without substrate bound.

The A264M/C/Q heme domains crystallize in the SB conformation, as seen for A264E and for palmitoleate- and other substrate-bound forms of WT BM3 heme domain [23,50]. The SB form is likely one of (at least) two major solution-state conformers of the BM3 heme domain, and possibly the conformer with higher affinity for fatty acids [22]. Coordination of heme iron by Met264 and Gln264 side chains clearly occurs in the SB conformer in the A264M/Q crystals. Apparent differences in proportions of the 6th ligand coordinated in these mutants between solution state, crystal and (low temperature) EPR forms may results from changes in the equilibrium of conformational states under these different conditions. Heterogeneity observed in the EPR spectra of A264M/C/Q mutants also suggests different ligation states and conformations of coordinating ligands. Covalent (oxidative) modification of the Cys264 side chain, which is too short to reach the heme iron in the SB conformation crystallized, might also occur (Figure 6). For A264M, the hydrophobic Met264 side chain could also interact with the ω-end of the fatty acid substrate (and least in the room temperature solution state) to enable development of HS heme iron.

CONCLUDING REMARKS

Our work reveals novel heme iron ligand sets, created by engineering heme iron coordinating residues at position 264 in the I helix region of P450 BM3. The first clear structural and/or spectroscopic evidence for Cys-Fe-Met and Cys-Fe-Gln heme iron ligation states is provided, and characterization of reduced forms of these species (and of other novel hexacoordinated species) is presented. The A264M/C/Q/E mutants retain fatty acid hydroxylase activity, although activity is diminished and NADPH oxidation is substantially uncoupled from laurate hydroxylation in all cases. The A264K/H mutants were inactive, consistent with essentially irreversible coordination of heme iron by Lys/His264 side chains. Substrate-dependent conversion of P450 heme iron to the HS form and laurate-dependent NADPH oxidation rate do not correlate well with rate of fatty acid hydroxylation in A264M/C/Q/E mutants, and lack of active site steric hindrance from the smaller Cys264 side chain may underlie the more efficient coupling of NADPH oxidation to substrate hydroxylation in the A264C enzyme. The A264M mutant has higher affinity than WT for fatty acids (lower K_d values), consistent with its co-purification with lipid (likely palmitate) from *E. coli*, as evident from its crystal structure. The combination of structural and spectroscopic analyses highlight differences in occupancy (and likely orientation for A264M) of the novel heme iron 6th ligands depending on temperature and solution, frozen or crystalline state of the proteins, which is likely testament to the different conformational states that can clearly be occupied by this P450.

In conclusion, our data present detailed structural/spectroscopic characterization of novel heme iron ligation sets in at least the A264M/Q mutants of BM3. In detailing the spectroscopic features of the BM3 A264 mutants, we provide data that will enable identification of such systems as and when they are observed in nature.

Acknowledgements

AWM wishes to thank the Royal Society for the award of a Leverhulme Trust Senior Research Fellowship. DL is a Royal Society University Research Fellow. The authors thank the Biotechnology and Biological Sciences Research Council (BBSRC) for financial support for their research.

References

[1] Munro, A.W., and Lindsay, J.G. (1996). Bacterial cytochromes P450. Mol. Microbiol. **20**, 1115-1125.

[2] Isin, E.M. and Guengerich, F.P. (2007). Complex reactions catalyzed by cytochrome P450 enzymes. Biochim. Biophys. Acta **1770**, 314-329.

[3] Munro, A.W., Girvan, H.M. and McLean, K.J. (2007). Variations on a (t)heme--novel mechanisms, redox partners and catalytic functions in the cytochrome P450 superfamily. Nat. Prod. Rep. **24**, 585-609.

[4] Denisov, I.G., Makris, T.M., Sligar, S.G. and Schlichting, I. (2005). Structure and chemistry of cytochrome P450. Chem. Rev. **105**, 2253-2267.

[5] Makris, T.M., von Koenig, K., Schlichting, I. and Sligar, S.G. (2006). The status of high-valent metal oxo complexes in the P450 cytochromes. J. Inorg. Biochem. **100**, 507-518.

[6] Munro, A.W., Girvan, H.M. and McLean, K.J. (2007). Cytochrome P450-redox partner fusion enzymes. Biochim. Biophys. Acta **1770**, 345-359.

[7] Davydov, R., Perera, R., Jin, S., Yang, T.C., Bryson, T.A., Sono, M., Dawson, J.H. and Hoffman, B.M. (2005). Substrate modulation of the properties and reactivity of the oxy-ferrous and hydroperoxo-ferric intermediates of cytochrome P450cam as shown by cryoreduction-EPR/ENDOR spectroscopy. J. Am. Chem. Soc. **127**, 1403-1413.

[8] Wang, M., Roberts, D.L., Paschke, R., Shea, T.M., Masters, B.S. and Kim, J.J. (1997). Three-dimensional structure of NADPH-cytochrome P450 reductase: prototype for FMN- and FAD-containing enzymes. Proc. Natl. Acad. Sci. USA **94**, 8411-8416.
[9] Paine, M.J.I., Scrutton, N.S., Munro, A.W., Gutierrez, A., Roberts, G.C.K. and Wolf, C.R. (2005). Electron transfer partners of cytochrome P450. Pp. 115-148 in Cytochrome P450 Structure, Mechanism and Biochemistry. Ed. Ortiz de Montellano, P.R. Published by Kluwer Academic/Plenum Publishers (New York).
[10] Puchkaev, A.V., Wakagi, T. and Oriz de Montellano, P.R. (2002). CYP119 plus a *Sulfolobus tokodaii* strain 7 ferredoxin and 2-oxoacid:ferredoxin oxidoreductase constitute a high-temperature cytochrome P450 catalytic system. J. Am. Chem. Soc. **124**, 12682-12683.
[11] Munro, A.W., Leys, D., McLean, K.J., Marshall, K.R., Ost, T.W., Daff, S., Miles, C.S., Chapman, S.K., Lysek, D.A., Moser, C.C., Page, C.C. and Dutton, P.L. (2002). P450 BM3: the very model of a modern flavocytochrome. Trends Biochem. Sci. 27, 250-257.
[12] Roitel, O., Scrutton, N.S. and Munro, A.W. (2003). Electron transfer in flavocytochrome P450 BM3: kinetics of flavin reduction and oxidation, the role of cysteine 999, and relationships with mammalian cytochrome P450 reductase. Biochemistry **42**, 10809-10821.
[13] Noble, M.A., Miles, C.S., Chapman, S.K., Lysek, D.A., MacKay, A.C., Reid, G.A., Hanzlik, R.P. and Munro, A.W. (1999), Roles of key active-site residues in flavocytochrome P450 BM3. Biochem. J. **339**, 371-379.
[14] Miles, J.S., Munro, A.W., Rospendowski, B.N., Smith, W.E., McKnight, J. and Thomson, A.J. (1992). Domains of the catalytically self-sufficient cytochrome P-450 BM-3. Genetic construction, overexpression, purification and spectroscopic characterization. Biochem. J. **288**, 503-509.
[15] Munro, A.W., Lindsay, J.G., Coggins, J.R., Kelly, S.M. and Price, N.C. (1994). Structural and enzymological analysis of the interaction of isolated domains of cytochrome P-450 BM3. FEBS Lett. **343**, 70-74.
[16] Peters, M.W., Meinhold, P., Glieder, A. and Arnold, F.H. (2003). Regio- and enantioselective alkane hydroxylation with engineered cytochromes P450 BM-3. J. Am. Chem. Soc. **125**, 13442-134540.
[17] Tee, K.L. and Schwaneberg, U. (2006). A screening system for the directed evolution of epoxygenases: importance of position 184 in P450 BM3 for stereoselective styrene epoxidation. Angew. Chem. Int. Ed. **45**, 5380-5383.
[18] Munro, A.W., Lindsay, J.G., Coggins, J.R., Kelly, S.M. and Price, N.C. (1996). Analysis of the structural stability of the multidomain enzyme flavocytochrome P-450 BM3. Biochim. Biophys. Acta **1296**, 127-137.
[19] LeBrun, L.A., Xu, F., Kroetz, D.L. and Ortiz de Montellano, P.R. (2002). Covalent attachment of the heme prosthetic group in the CYP4F cytochrome P450 family. Biochemistry **41**, 5931-5937.
[20] Baer, B.R., Kunze, K.L. and Rettie, A.E. (2007). Mechanism of formation of the ester linkage between heme and Glu310 of CYP4B1: ^{18}O protein labeling studies. Biochemistry **46**, 11598-11605.
[21] Limburg, J., LeBrun, L.A. and Ortiz de Montellano. P.R. (2005). The P450cam G248E mutant covalently binds its prosthetic heme group. Biochemistry **44**, 4091-4099.
[22] Girvan, H.M., Marshall, K.R., Lawson, R.J., Leys, D., Joyce, M.G., Clarkson, J., Smith, W.E., Cheesman, M.R., and Munro, A.W. (2004). Flavocytochrome P450 BM3 mutant A264E undergoes substrate-dependent formation of a novel heme iron ligand set. J. Biol. Chem. **279**, 23274-23286.
[23] Joyce, M.G., Girvan, H.M., Munro, A.W. and Leys, D. (2004). A single mutation in cytochrome P450 BM3 induces the conformational rearrangement seen upon substrate binding in the wild-type enzyme. J. Biol. Chem. **279**, 23287-23293.
[24] Girvan, H.M., Seward, H.E., Toogood, H.S., Cheesman, M.R., Leys, D. and Munro, A.W. (2007). Structural and spectroscopic characterization of P450 BM3 mutants with unprecedented P450 heme

iron ligand sets. New heme ligation states influence conformational equilibria in P450 BM3. J. Biol. Chem. **282**, 564-572.
[25] Neeli, R., Roitel, O., Scrutton, N.S. and Munro, A.W. (2005). Switching pyridine nucleotide specificity in P450 BM3: mechanistic analysis of the W1046H and W1046A enzymes. J. Biol. Chem. **280**, 17634-17644.
[26] Berry, E.A. and Trumpower, B.L. (1987). Simultaneous determination of hemes a, b, and c from pyridine hemochrome spectra. Anal. Biochem. **161**, 1-15.
[27] Neeli, R., Girvan, H.M., Lawrence, A., Warren, M.J., Leys, D., Scrutton, N.S. and Munro, A.W. (2005). The dimeric form of flavocytochrome P450 BM3 is catalytically functional as a fatty acid hydroxylase. FEBS Lett. **579**, 5582-5588.
[28] Lawson, R.J., Leys, D., Sutcliffe, M.J., Kemp, C.A,, Cheesman, M.R., Smith, S.J., Clarkson, J., Smith, W.E., Haq, I., Perkins, J.B. and Munro, A.W. (2004). Thermodynamic and biophysical characterization of cytochrome P450 BioI from *Bacillus subtilis*. Biochemistry **43**, 12410-12426.
[29] Dutton, P.L. (1978). Redox potentiometry: Determination of midpoint potentials of oxidation-reduction components of biological electron-transfer systems. Methods Enzymol. **54**, 411-435.
[30] Daff, S.N., Chapman,S.K., Turner, K.L., Holt, R.A., Govindaraj, S., Poulos, T.L. and Munro, A.W. (1997). Redox control of the catalytic cycle of flavocytochrome P-450 BM3. Biochemistry **36**, 13816-13823.
[31] Collaborative Computational Project, Number 4. (1994) The CCP4 Suite: Programs for Protein Crystallography. Acta Crystallogr. **D50**, 760-763.
[32] Murshudov, G.N. Vagin, A.A. and Dodson, E.J. (1997). Refinement of Macromolecular Structures by the Maximum-Likelihood Method. Acta Crystallogr. **D53**, 240-255.
[33] Emsley, P. and Cowtan, K. (2004) Coot: model-building tools for molecular graphics. Acta Crystallogr. **D60**, 2126-2132.
[34] McLean, K.J., Warman, A.J., Seward, H.E., Marshall, K.R., Girvan, H.M., Cheesman, M.R., Waterman, M.R. and Munro, A.W. (2006). Biophysical characterization of the sterol demethylase P450 from *Mycobacterium tuberculosis*, its cognate ferredoxin, and their interactions. Biochemistry **45**, 8427-8443.
[35] Perera, R., Sono, M., Sigman, J.A., Pfister, T.D., Lu, Y. And Dawson, J.H. (2003). Neutral thiol as a proximal ligand to ferrous heme iron: implications for heme proteins that lose cysteine thiolate ligation on reduction. Proc. Natl. Acad. Sci. USA **100**, 3641-3646.
[36] Dunford, A.J., McLean, K.J., Sabri, M., Seward, H.E., Heyes, D.J., Scrutton, N.S. and Munro, A.W. (2007). Rapid P450 heme iron reduction by laser photoexcitation of *Mycobacterium tuberculosis* CYP121 and CYP51B1. Analysis of CO complexation reactions and reversibility of the P450/P420 equilibrium. J. Biol. Chem. **282**, 24816-24824.
[37] Quaroni, L.G., Seward, H.E., McLean, K.J., Girvan, H.M., Ost, T.W., Noble, M.A., Kelly, S.M., Price, N.C., Cheesman, M.R., Smith, W.E. and Munro, A.W. (2004). Interaction of nitric oxide with cytochrome P450 BM3. Biochemistry **43**, 16416-16431.
[38] Yeom, H., Sligar, S.G., Li, H., Poulos, T.L. and Fulco, A.J. (1995). The role of Thr268 in oxygen activation of cytochrome P450BM-3. Biochemistry **34**, 14733-14740.
[39] Ost, T.W., Miles, C.S., Munro, A.W., Murdoch, J., Reid, G.A. and Chapman, S.K. (2001). Phenylalanine 393 exerts thermodynamic control over the heme of flavocytochrome P450 BM3. Biochemistry **40**, 13421-13429.
[40] Sono, M., Andersson, L.A. and Dawson, J.H. (1982). Sulfur donor ligand binding to ferric cytochrome P450cam and myoglobin. Ultraviolet-visible absorption, magnetic circular dichroism, and electron paramagnetic resonance spectroscopic investigations of the complexes. J. Biol. Chem. **257**, 8308-8320.

[41] Sono, M., Hager, L.P. and Dawson, J.H. (1991). Electron paramagnetic resonance investigations of exogenous ligand complexes of low-spin ferric chloroperoxidase: further support for endogenous thiolate ligation to the heme iron. Biochim. Biophys. Acta **1078**, 351-359.
[42] Cheesman, M.R., Little, P.J. and Berks, B.C. (2001). Novel heme ligation in a *c*-type cytochrome involved in thiosulfate oxidation: EPR and MCD of SoxAX from *Rhodovulum sulfidophilum*. Biochemistry **40**, 10562-10569.
[43] Cheesman, M.R., Thomson, A.J., Greenwood, C., Moore, G.R. and Kadir, F. (1990). Bis-methionine axial ligation of haem in bacterioferritin from *Pseudomonas aeruginosa*. Nature **346**, 771-773.
[44] McKnight, J., Cheesman, M.R., Thomson, A.J., Miles, J.S. and Munro, A.W. (1993). Identification of charge-transfer transitions in the optical spectrum of low-spin ferric cytochrome P-450 *Bacillus megaterium*. Eur. J. Biochem. **213**, 683-687.
[45] Spiro, T.G. (1985). Resonance Raman spectroscopy as a probe of heme-protein structure and dynamics. Adv. Prot. Chem. **37**, 111-159.
[46] Abe, M., Kitagawa, T. and Kyogoku, Y. (1978). Resonance Raman spectra of octaethylporphyrinato-Ni(III) and meso-deuterated and N15-substituted derivatives 2. Normal coordinate analysis. J. Phys. Chem. **69**, 4526-4534.
[47] Smith, S.J., Munro, A.W. and Smith, W.E. (2003). Resonance Raman scattering of cytochrome P450 BM3 and effect of imidazole inhibitors. Biopolymers **70**, 620-627.
[48] Hildebrandt, P., Greinert, R., Stier, A. and Taniguchi, H. (1989). Resonance Raman study on the structure of the active sites of microsomal cytochrome P-450 isozymes LM2 and LM4. Eur. J. Biochem. **186**, 291-302.
[49] Lee, D.S., Yamada, A., Sugimoto, H., Matsunaga, I., Ogura, H., Ichihara, K., Adachi, S., Park, S.Y. and Shiro, Y. (2003). Substrate recognition and molecular mechanism of fatty acid hydroxylation by cytochrome P450 from *Bacillus subtilis*. Crystallographic, spectroscopic, and mutational studies. J. Biol. Chem. **278**, 9761-9767.
[50] Li, H.Y. and Poulos, T.L. (1997). The structure of the cytochrome P450BM-3 haem domain complexed with the fatty acid substrate, palmitoleic acid. Nature Struct. Biol. **4**, 140-146.
[51] Sundaramoorthy, M., Choudhury, K., Edwards, S.L. and Poulos, T.L. (1991). Crystal structure and preliminary functional analysis of the cytochrome *c* peroxidase Hisl75Gln proximal ligand mutant. J. Am. Chem. Soc. **113**, 7755-7757.
[52] Leys, D., Backers, K., Meyer, T.E., Hagen, W.R., Cusanovich, M.A. and Van Beeumen, J.J. (2000). Crystal structures of an oxygen-binding cytochrome *c* from *Rhodobacter sphaeroides*. J. Biol. Chem. **275**, 16050-16056.

Tables

Table 1. Kinetic parameters for fatty acid oxidation by WT and A264 mutant flavocytochromes P450 BM3. Data were collected as described in the *Experimental* section. The k_{cat} data indicated with asterisks are second order rate constants expressed in units of μM^{-1} min^{-1} with respect to fatty acid concentration. ND indicates "not determinable" for mutants in which fatty acid binding did not induce any significant perturbation of heme iron optical properties. WT data for arachidonic acid oxidation kinetics are from reference 12. Data for fatty acid oxidation kinetics and binding for the A264E mutant are from reference 22.

Table 2. Heme iron redox potentials for WT and A264 mutant BM3 heme domains. Heme iron potentials were determined as described previously and for substrate-free and arachidonate-bound proteins [22,30]. Data are midpoint reduction potentials relative to the standard hydrogen electrode (SHE). Data for the A264E mutant are from reference 22. ND indicates not determined for the A264K/H mutants, for which no modulation of heme spectrum was observed on binding of fatty acids.

BM3 Enzyme	Fatty acid substrate					
	Lauric acid			Arachidonic acid		
	k_{cat} (min^{-1})	K_M (μM)	K_d (μM)	k_{cat} (min^{-1})	K_M (μM)	K_d (μM)
WT	2770 ± 120	87.4 ± 8.1	89 ± 15	16400 ± 185	5.1 ± 0.4	0.55 ± 0.05
A264H	0.25 ± 0.07*		ND	0.89 ± 0.21*		ND
A264K	0.36 ± 0.07*		ND	3.13 ± 1.64*		ND
A264Q	1.92 ± 0.17*		ND	754 ± 14	1.86 ± 0.46	18 ± 1.5
A264M	195 ± 5	5.2 ± 0.8	17.8 ± 0.9	115 ± 4	10.3 ± 1.5	0.35 ± 0.02
A264C	0.08 ± 0.01*		ND	0.56 ± 0.05*		6.4 ± 0.3
A264E	744 ± 21	114 ± 12	ND	2770 ± 120	87 ± 8	100 ± 15

Table 1

P450 BM3 heme domain	Redox Potential (mV vs. SHE)	
	Substrate-free	Arachidonate-bound
WT	-392 ± 5	-283 ± 4
A264H	-412 ± 8	ND
A264K	-420 ± 8	ND
A264Q	-396 ± 5	-35 ± 4
A264M	-220 ± 8	-227 ± 7
A264C	-385 ± 5	-240 ± 6

Table 2

Figures

Figure 1. Optical properties of P450 BM3 heme domain and A264 mutants. Panel A shows UV-visible absorption spectra for WT (dotted line), A264H (thick solid line), A264Q (dashed line) and A264M (thin solid line) heme domains. Proteins are at a concentration of ~5 μM. Soret absorption maxima are at 418 nm, 427 nm, 418 nm and 416 nm, respectively. Inset shows magnified image of Soret maxima. Panel B shows optical spectra for purified A264M heme domain (8 μM, thick solid line) and when bound to arachidonic acid (52.8 μM, thin solid line). Inset shows selected optical difference spectra from the titration, with difference spectra shown (of increasing magnitude) at substrate concentrations of 3.3, 6.6, 9.9, 19.8, 29.7 and 52.8 μM. Peak and trough in the difference spectra are at 421 and 389 nm, respectively.

Figure 2. Inhibitor binding to P450 BM3 A264 heme domain mutants. Panel A shows selected UV-visible absorption spectra for the titration of the A264C heme domain (2.5 μM) with 4-PIM (the most intense spectrum is prior to 4-PIM addition, successive spectra of decreasing intensity are at 10, 20, 40, 50 and 100 μM 4-PIM). The Soret shift is from 418 to 422.5 nm. The inset shows the 4-PIM-induced optical shift ($A_{435} - A_{415}$ nm) data fitted to a hyperbolic function (K_d = 52.0 ± 2.8 μM). Panel B shows the absorption spectrum for the A264Q heme domain (6.5 μM) in its oxidised, ligand-free form (thin, solid line), in complex with NO (dashed line) and in its reduced, CO-bound state (thick, solid line). Soret maxima for these species are at 418, 433.5 and 448 nm, respectively.

Figure 3. Potentiometric analysis of P450 BM3 A264C and A264M heme domains. Panel A shows selected UV-visible absorption spectra collected during redox titration of the substrate-free form of A264C heme domain (7.5 μM). The spectrum for oxidised heme domain is shown as a thick solid line, and the spectrum for the reduced enzyme as a dashed line. Intermediate spectra are in thin solid lines. Arrows indicate directions of absorption change during the reductive phase of the titration at different points in the spectrum. The inset shows a plot of heme absorption (A_{390}) versus applied potential, with data fitted to the Nernst function to produce a midpoint reduction potential of E = -385 ± 5 mV (vs. the standard hydrogen electrode, SHE). Panel B shows a comparable data set for the arachidonate-bound form of the A264M heme domain (9.4 μM). Arrows again indicate direction of absorption changes on heme reduction. Inset shows a fit of A_{398} data to applied potential (as in panel A), yielding E = -227 ± 7 mV.

Figure 4. **Determination of pK_a for the P450 BM3 A264K heme domain**. The main panel shows selected spectra for the dithionite-reduced A264K heme domain (4.2 μM MTE buffer - 50 mM MES, 25 mM Tris, 25 mM ethanolamine, starting pH 5.45) collected at various pH values from 5.45 (thin, solid line) to 8.80 (bold, solid line) on titration with sodium hydroxide. The Soret feature is at 423 nm at pH 5.5, and as pH is increased this band decreases in intensity and a second feature (peak at 445 nm) becomes prominent. Intermediate spectra (shown as dashed lines) were collected at pH 5.90, 6.13, 6.31, 6.54, 6.80, 7.08 and 8.04. Arrows indicate direction of absorption change with increasing pH at key wavelengths. The inset shows a plot of A_{425} data versus pH, with a single pK_a function used to fit the data, producing a pK_a value of 6.50 ± 0.04 for the thiol/thiolate transition of the heme cysteine ligand.

Figure 5. **Perpendicular mode EPR spectra of WT and A264 mutant P450 BM3 heme domains at X-band frequency**. The spectra for WT and A264C/M/Q BM3 heme domains are overlaid, and g-values are indicated for features in each of the spectra. Microwave power was 2 milliwatts, modulation amplitude 10 G, temperature 10.8 K, and proteins were at concentrations 400 μM (WT), 450 μM (A264C), 520 μM (A264M) and 745 μM (A264Q).

Figure 6. **Heme binding site structure in the A264M/C/Q heme domains**. Panel A shows heme environment in the A264C domain. Cysteinate proximal ligand (C400) is retained and the Cys264 residue occupies active site space above the heme plane, but without interacting directly with the heme iron. A water molecule is retained as 6th ligand to the heme iron. Positions of the catalytically important Phe87 and Thr268 residues are shown. Corresponding electron density is contoured at 1σ and shown as a blue mesh here and for structures in panels B and C. Panel B shows a similar image for the A264M heme domain. In this case Met264 coordinates the heme iron and the distal water is displaced. A fatty acid molecule (modelled as palmitate) is bound and interacts with the Phe87 side chain. Panel C shows the structure of the A264Q heme domain. Gln264 is present in two conformations. The ligating conformation is modelled coordinating to the heme iron via its amide oxygen atom. The second Gln264 conformation is distant from the heme and interacts with the 6th ligand water molecule.

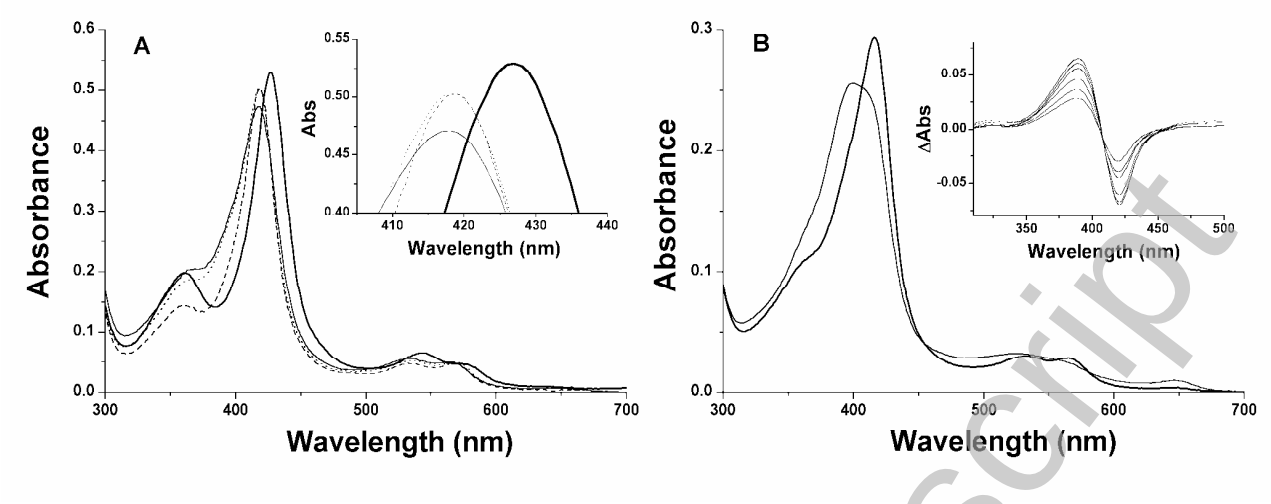

Figure 1

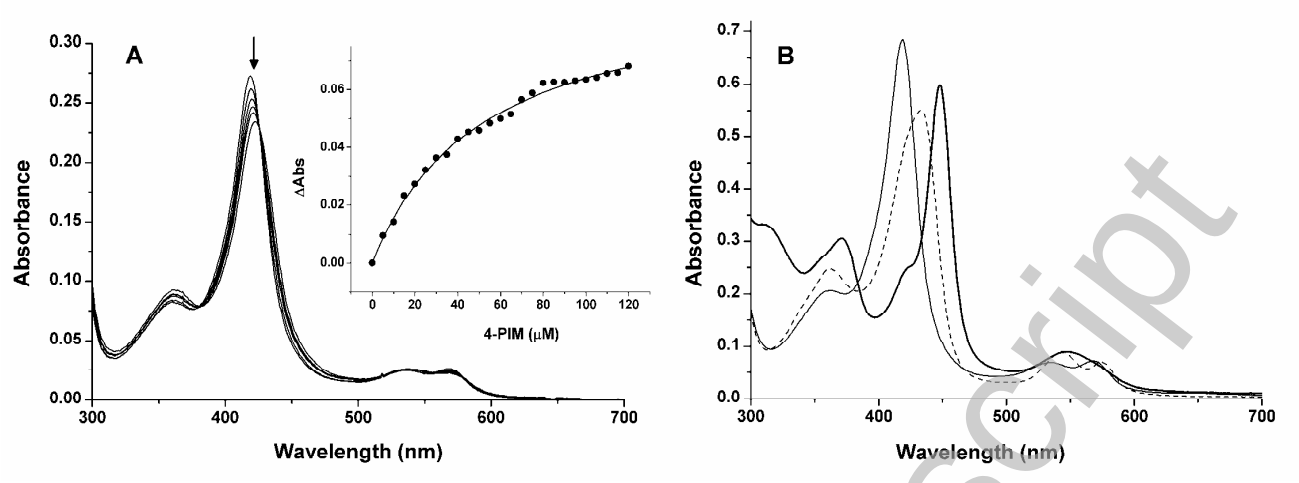

Figure 2

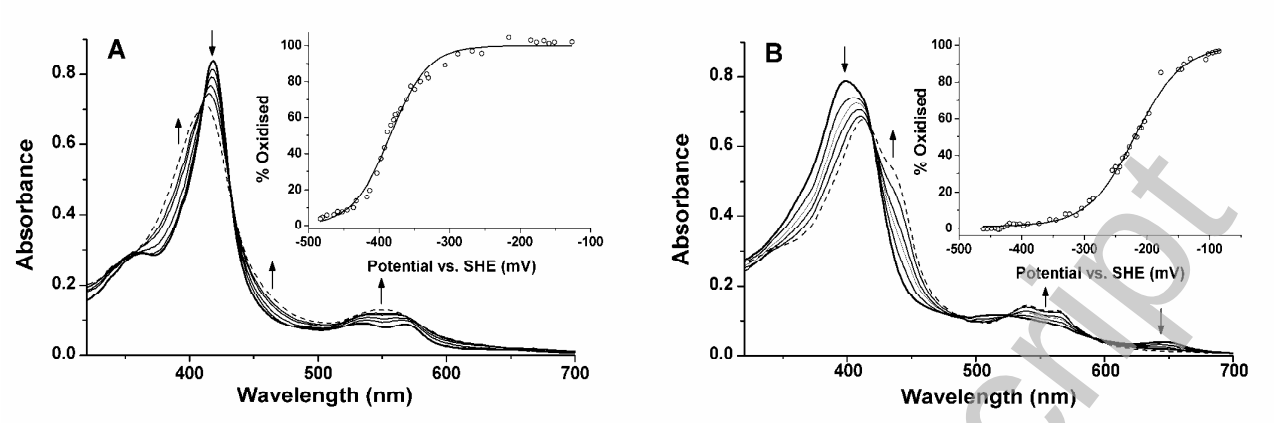

Figure 3

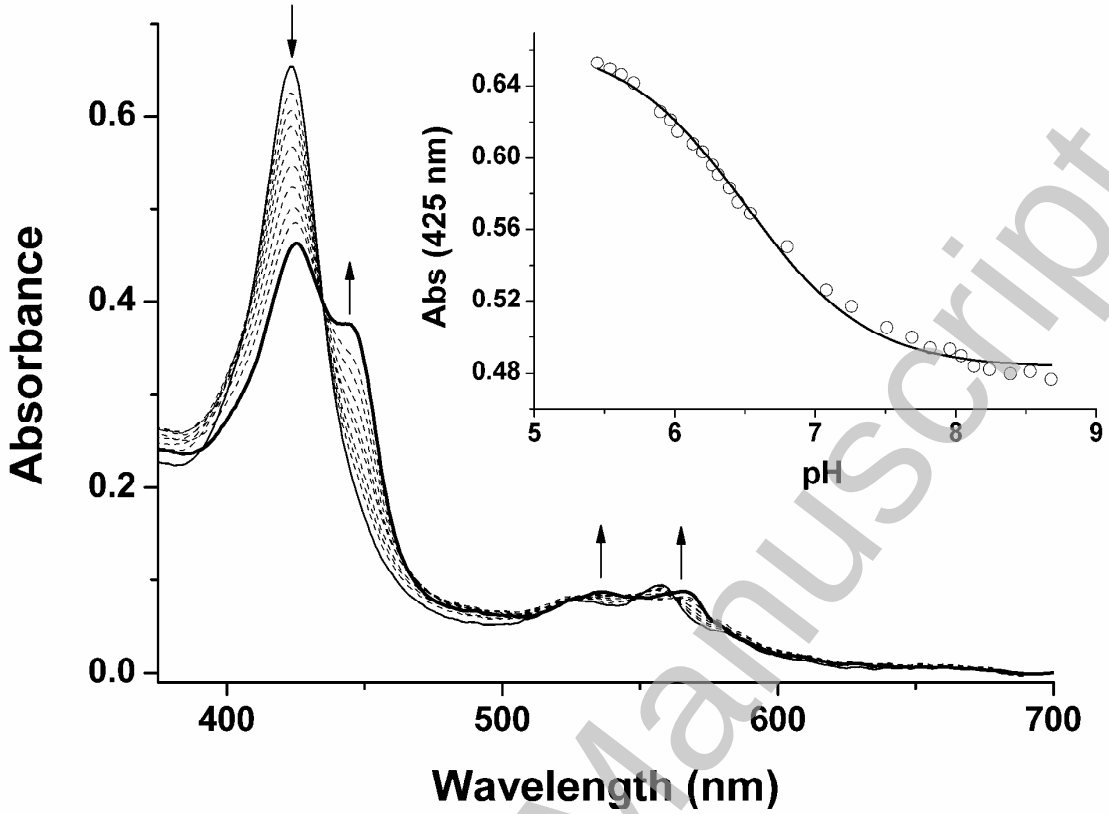

Figure 4

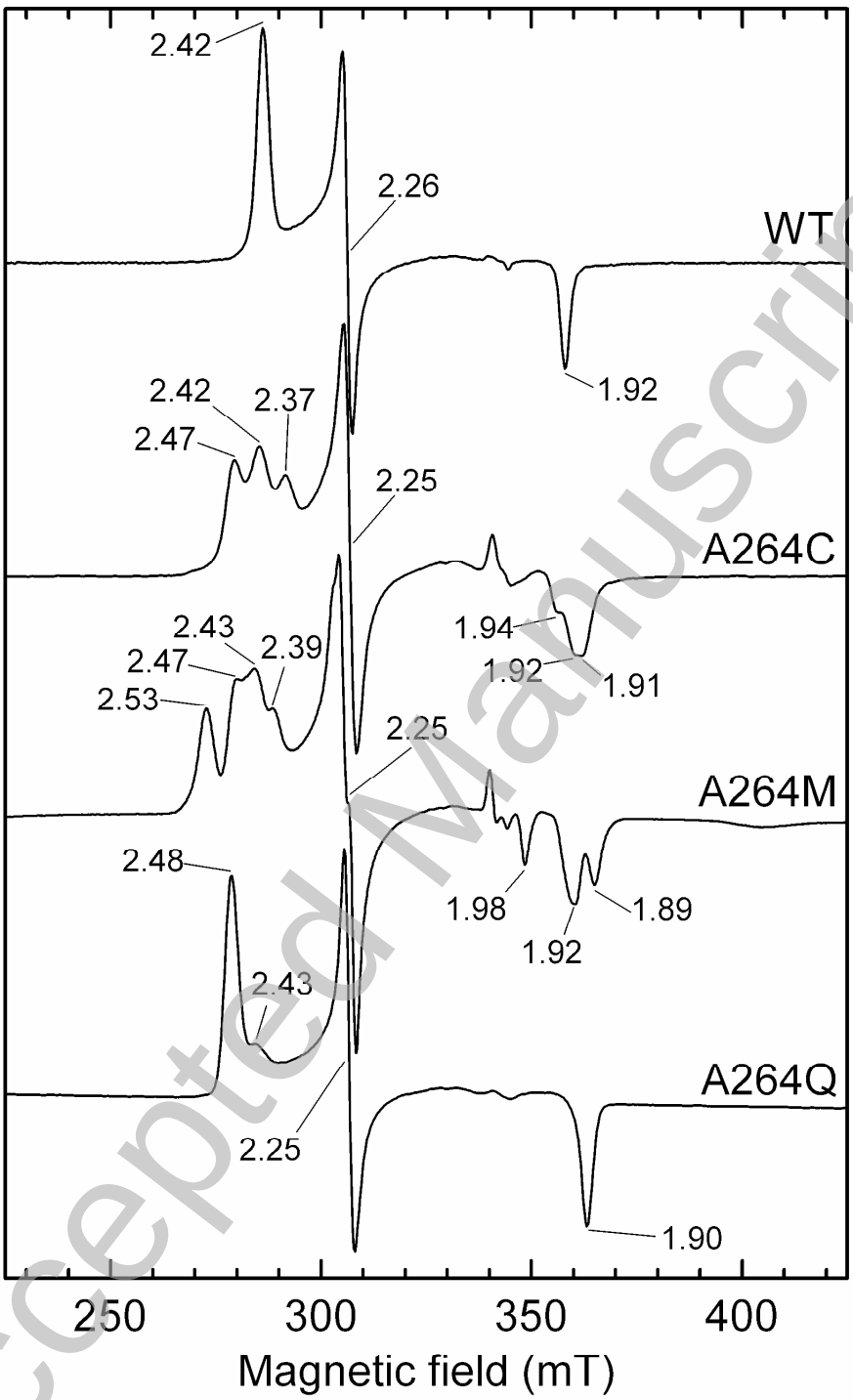

Figure 5

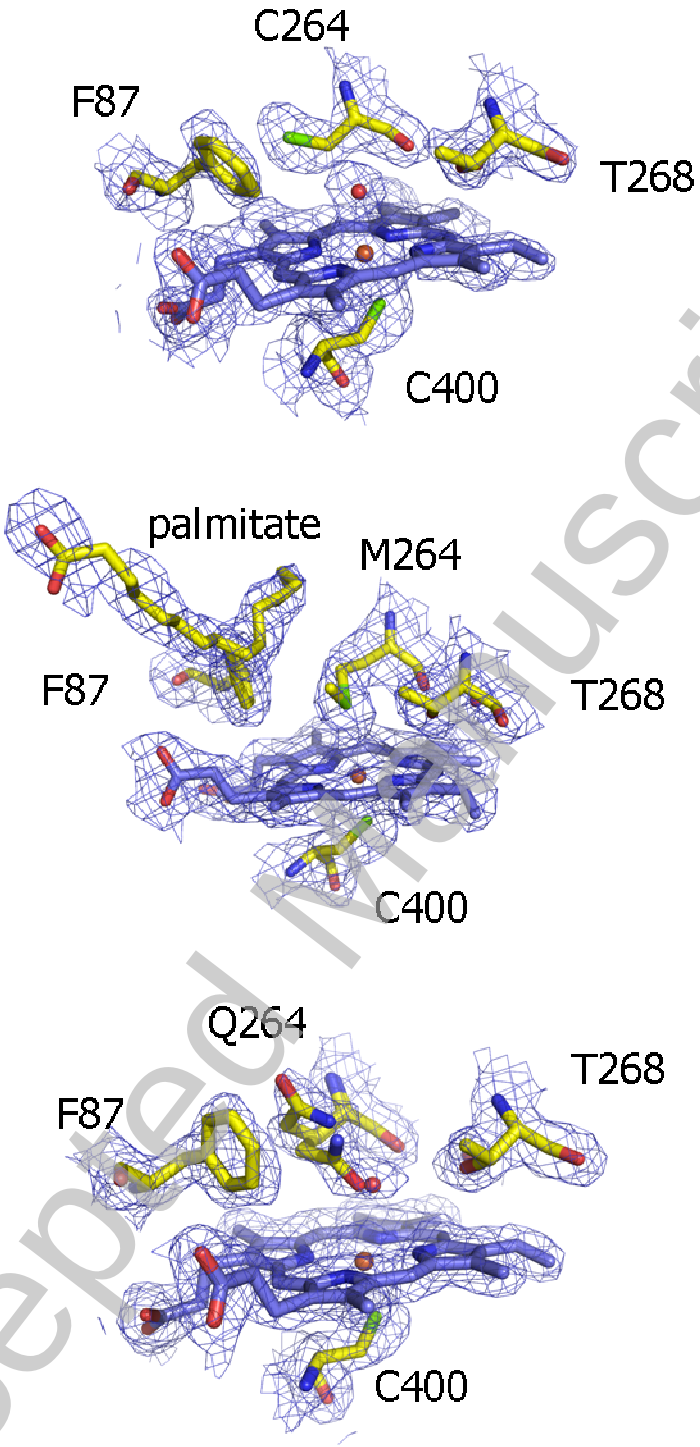

Figure 6